tion of surface plasmon resonances in metal (usually gold or silver) nanostructures formed (e.g., deposited) on the surface of SERS substrates [13]; and 2) the mechanism of chemical amplification [14], where electrons tunnel from metal nanostructures into analyte molecules, thereby changing the electronic structure of the molecule–metal nanoparticle system and, accordingly, the polarization of molecules.

To realize effective amplification of the Raman signal from analytes, both local surface plasmon resonances (LSPRs) [13], which are excited in metal nanoparticles or rough metal film irregularities, and surface plasmon polaritons (SPPs) [15] are used. The latter are excited at the surface of metal films using prisms in the Kretschmann and Otto configuration [16] or periodic one-dimensional or binary structures (gratings) with a metal film deposited on their surface. It is worth noting that the Kretschmann and Otto techniques [16] are used more often, because the application of prisms makes the implementation of resonance excitation conditions easier and, finally, cheaper as compared with gratings. On the other hand, by varying the grating parameters, namely, its period a and the relief modulation depth h/a, where h is the ridge height, it is possible to choose the conditions under which the LSPR and the SPP resonance will be realized simultaneously or to achieve the required surface plasmon excitation angle.

Another important point concerning providing conditions for effective amplification of various analytes is the creation of a large number of the so-called "hot spots" on SERS substrates. The research of SERS mechanisms [17] showed that, in many cases, the main contribution to the amplification of the Raman signal from analytes is given just by hot spots. Thus, it can be asserted that the efficiency of SERS spectroscopy depends mainly on the morphology of the partially or completely metalized SERS substrate surface onto which the analyzed substances are deposited. Moreover, for the application of SERS to be effective, it is necessary to develop substrates that would be characterized by chemical stability, a high amplification factor, lateral homogeneity, and relative ease of manufacture.

Nowadays, many various types of SERS substrates are known. The most widespread of them are based on laterally ordered [18] or disordered [19,20] arrays of silver or gold nanoparticles deposited onto dielectric wafers. However, their fabrication, as a rule, requires a high-tech equipment and is rather expensive. SERS substrates in the form of plates with a surface relief can be cheaper; they can be replicated by stamping and afterward covered with a metal layer. The simplest technology for the manufacture of such plates with a required surface relief is interference lithography. In our previous studies, it was shown that this technology with the application of high-resolving chalcogenide photoresist is promising for the formation of one- and two-dimensional submicronic periodic structures on the surface of semiconductors and insulators [21]. Wafers with the surface relief of two types can be used as SERS substrates: in the form of laterally ordered arrays of either cavities (holes) or bumps (domes); see Fig. 1. Depending on the morphologic parameters of such structures (the spatial period and the modulation depth), LSPRs and/or SPPs can be excited in them.

In this work, a comparative study is performed concerning the SERS parameters of the substrates of those two types, as well as their efficiency of Raman signal amplification on the standard R6G analyte.

2. Experimental Part

Laterally ordered relief structures for SERS substrates were formed by means of the interference photolithography method and applying a two-layer chalcogenide photoresist [22]. An adhesive Cr layer 30 nm in thickness, a relief-forming layer of $As_{10}Ge_{30}S_{60}$ 700 nm in thickness, and a photosensitive layer of $As_{40}S_{30}Se_{30}$ 100 nm in thickness were successively deposited onto polished glass plates using the thermal evaporation in a vacuum of 2×10^{-3} Pa. The thickness of the layers was monitored with the help of a quartz thickness gauge KIT-1 during the film deposition, and with the help of an MII-4 microinterferometer after the deposition.

The interference structures on the $As_{40}S_{30}Se_{30}$ film were registered using the interference patterns obtained from the radiation of a helium-cadmium laser (λ = 441.6 nm). When registering two-dimensional matrices of holes or domes, a double scanning of specimens was carried out. Before the second scanning, the specimen was rotated by 90° around the normal to its surface. After the scanning process, the selective liquid etching of the $As_{40}S_{30}Se_{30}$ layer was carried out in order to form a lithographic mask with holes (their size depended on the etching time) that reached the surface of the $As_{10}Ge_{30}S_{60}$ layer. At this stage, the se-

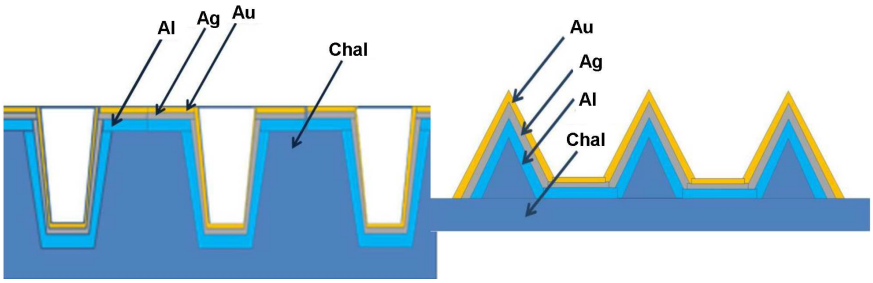

Fig. 1. Schematic images of formed reliefs on SERS substrates of two types: with holes (*a*) and with domes (*b*). Designations: Chal is a relief-forming $As_{10}Ge_{30}S_{60}$ layer 700 nm in thickness, Al is an aluminum layer 80 nm in thickness, Ag is a silver layer 70 nm in thickness, and Au is a gold layer 10 nm in thickness

lective etchant of photoresist $As_{40}S_{30}Se_{30}$ was used, which did not dissolve the relief-forming $As_{10}Ge_{30}S_{60}$ layer.

The next stage included the relief formation by etching through the holes in the lithographic mask, but in a solvent for $As_{10}Ge_{30}S_{60}$ that did not dissolve the photoresist. The shape of the elements in the obtained periodic structures (holes or domes) was mainly determined by the etching time at this stage of the technological process. Etching of the photoresist and the relief-forming layer was monitored *in situ* by registering the non-photoactive longwave radiation diffracted from the relief structure. After removing the remnants of the $As_{40}S_{30}Se_{30}$ photoresist, washing and drying the specimens, formed periodic $As_{10}Ge_{30}S_{60}$-based structures were obtained.

The obtained periodic structures were covered with an Al layer 80 nm in thickness, which was then covered with an opaque 70-nm Ag layer and a 10-nm Au layer (the indicated metal layers were deposited using the method of thermal deposition in vacuum); see Fig. 1. The aluminum layer was deposited in order to prevent the diffusion of silver into the relief-forming chalcogenide layer and its subsequent interaction with the latter. Deposition of the thin gold layer prevented the oxidation of silver during the measurements. The manufacturing technique of such structures was described in more details in our work [23].

To determine the profile shape and the size of the relief elements in the obtained periodic structure, a Dimension 3000 Scanning Probe atomic force microscope (Digital Instruments Inc., Tonawanda, NY, USA) was used. The spatial frequency of periodic relief structures was determined with an accuracy of ± 1 line/mm on an optical stand based on a G5M goniometer.

The optical properties of manufactured structures were studied by measuring the spectral-angular dependences of the polarized light reflection in a wavelength interval of 0.4–1.1 μm and for incidence angles within an interval of 10–70°. The automated installation for performing such measurements consisted of an illuminator, a mechanical light modulator, a monochromator with a Glahn prism at its output, and a rotary stage for specimens. The intensity of the light specularly reflected from a specimen was measured by means of a silicon photodetector, whose output signal, after the amplification and demodulation, was fed to the input of an analog-to-digital converter. Such spectrometric measurements made at several angles of light incidence allow the dispersion dependences of excited optical modes to be plotted and their nature to be identified.

The specular reflection spectra of the specimens at the normal light incidence were studied on a StellarNet Silver Nova 25 BWI6 spectrometer. Raman spectra were excited by the radiation emitted from solid-state lasers with wavelengths of 457, 532, and 671 nm and registered on a single-stage spectrometer MDR-23 (LOMO) equipped with a cooled CCD detector (Andor iDus 420, UK). In order to prevent heat-induced modifications of the specimens during their research, the power density of laser radiation at the specimens was lower than 10^3 W/cm^2. The spectral resolution of the spectrometer was determined using the width of the phonon band from a monocrystalline silicon substrate, and it amounted to 3 cm^{-1}. The frequency position of the phonon band from Si (521.0 cm^{-1}) was applied as a ref-

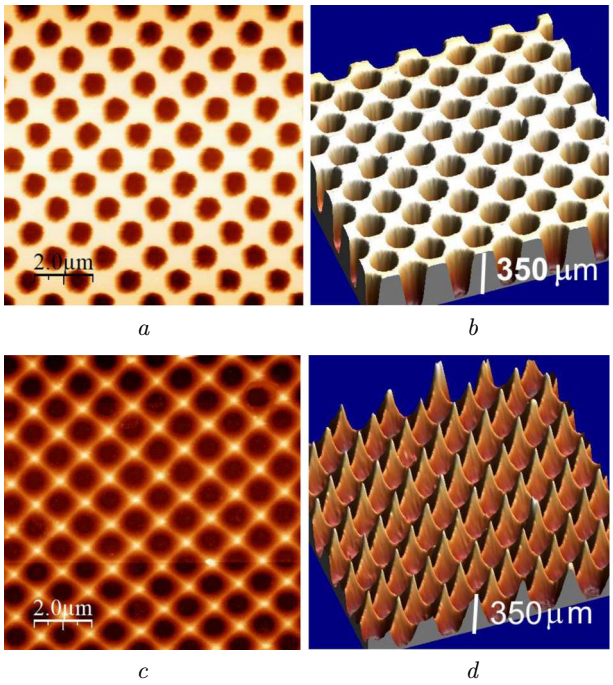

Fig. 2. AFM images of researched SERS substrates: specimen with holes (top view) (*a*), specimen with holes (side view) (*b*), specimen with domes (top view) (*c*), and specimen with domes (side view) (*d*)

erence while determining the frequency positions of other Raman bands.

3. Results and Their Discussion

Figure 2 demonstrates an AFM image of two SERS substrates with the surface relief in the form of laterally ordered arrays of holes (panels *a* and *b*) and domes (panels *c* and *d*). Both SERS substrates have the same spatial arrangement period of elements in mutually perpendicular directions, which is equal to 1200 ± 1 nm (the spatial frequency $\nu = 833$ mm^{-1}). The difference is that the etching time of the relief-forming $As_{10}Ge_{30}S_{60}$ layer for the specimen whose surface morphology is shown in Figs. 2, *a* and 2, *b* was 8 min, and that for the specimen with domes (Figs. 2, *c* and 2, *d*) was 15 min, which led to the formation of reliefs with different shapes. For the illustrated SERS substrates (Figs. 2, *a* and 2, *b*), the relief depth $h \approx 350$ nm, and the ratio between the relief depth and the structure period d (the relief modulation depth) equals $h/a \approx 0.33$.

As was shown by AFM studies, the deposition of metal layers [aluminum (80 nm), silver (70 nm), and

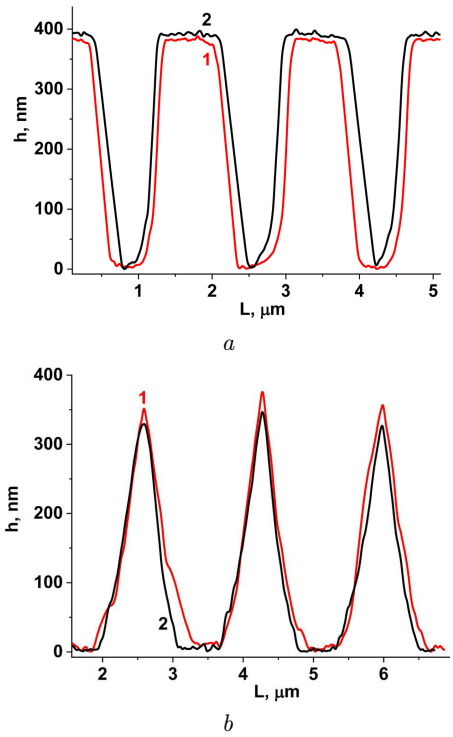

Fig. 3. Reliefs of formed structures before (curves *1*) and after (curves *2*) the the sputtering deposition of metal layers: with holes (*a*) and with domes (*b*)

gold (10 nm)] decreased the width of the holes by 10–15%, with the relief depth remaining almost unchanged (Fig. 3, *a*). As for the domes, their height increased by 10–15%, whereas the lateral dimensions increased by only 5% (Fig. 3, *b*).

As mentioned above, the Al film 80 nm in thickness prevented the silver atoms from penetrating into the chalcogenide layer and reacting with it. The next layer (70-nm, silver) covering the aluminum one played a major role in the excitation of plasmon resonances – in particular, LSPRs – in the holes and the domes' tops, as well as SPPs at the surface of the periodically profiled silver film. The top layer (10-nm, gold) played a dual role. On the one hand, it was a protective layer that did not allow silver to be oxidized; on the other hand, it slightly shifted the plasmon absorption band toward the long-wavelength region. It is important to note that both LSPR and SPP excitation are possible in such metalized periodic structures.

With regard for the sufficient total thickness of the metal layers on the surface of examined structures

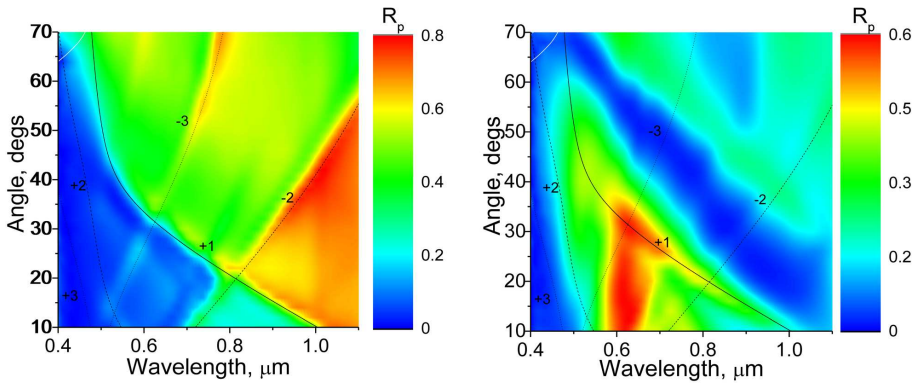

Fig. 4. Spectral-angular dependences of the light reflection by a periodic binary structure of holes (a) and domes (b) with a period of 1200 nm, with superimposed dispersion dependences of surface plasmon-polariton modes at the air/silver interface calculated for $m = +1$, -2, $+2$, and -3

(∼160 nm), plasmon resonances can be excited only at the metal layer-air interface, if the specimen is illuminated from the metal side. The condition for the SPP excitation is the conservation of the quasi-momentum with making allowance for the components of the wave vectors of incident radiation ($k_0 = 2\pi/\lambda$, where λ is the incident radiation wavelength) and plasmon-polaritons (k_{SPP}) that are parallel to the surface of the periodic structure, as well as the reciprocal structure vector ($G = 2\pi/a$, where a is the spatial period of the structure). The researched structures (see Fig. 2) were matrices symmetric with respect to the rotation by 90° and consisting of mutually perpendicular rows of holes (or domes). If the incidence plane of p-polarized excitation radiation is oriented perpendicularly (in parallel) to those substrate rows, the SPP excitation condition can be written in the scalar form as follows [24]:

$$\mathrm{Re}\ k_{\mathrm{SPP}} = nk_0 \sin\theta \pm mG, \qquad (1)$$

where Re k_{SPP} is the real part of k_{SPP}, θ is the light incidence angle, m is an integer number ($m \neq 0$) denoting the SPP diffraction order, and n is the refractive index of the environment.

For an approximate estimate of the SPP wave vector value, the expression obtained for the flat interface between semiinfinite media is often used [24]. In this approximation, formula (1) makes it possible to determine the incidence angle at which the SPPs are excited at a given incident radiation wavelength, i.e., to plot the $\theta(\lambda)$ dispersion dependences for SPPs excited at the metal/air interface. In the calculations, the optical constants of silver were taken from work [25].

The excitation of SPPs in relief periodic structures (gratings or bigratings) with a small relief modulation depth (h/a <0.2) manifests itself as a minimum in the angular or spectral dependence of specular reflection [26]. For structures with larger h/a-values (as for our both examined specimens), this minimum "degrades", and the plasmon resonance can manifest itself in the form of a sharp variation of the reflection value or its maximum.

Figure 4 demonstrates the measurement results obtained for the spectral-angular dependences of the specular reflection R_p of p-polarized radiation from the studied SERS substrates in the form of matrices of holes (panel a) and domes (panel b). The plane of radiation incidence at those measurements was oriented perpendicularly (in parallel) to the rows formed in the SERS substrates. From Fig. 4, a, one can see that the SPP excitation of orders $+1$, -2, and $+2$ was observed for the specimen with holes. Some deviations of the calculated curves from the experimental results are associated with the application of the "shallow relief" approximation in the calculations and with the neglect of the influence of the thin Au layer (10 nm) that covered the Ag one (70 nm).

The matrix of domes (Fig. 4, b) demonstrated only the SPP excitation of the order $+1$ in the restricted spectral-angular interval ($0.6\ \mu\mathrm{m} \leq \lambda \leq 1\ \mu\mathrm{m}$, $10° \leq \theta \leq 37°$). In addition, in the same angular interval, one can observe an intensive reflection

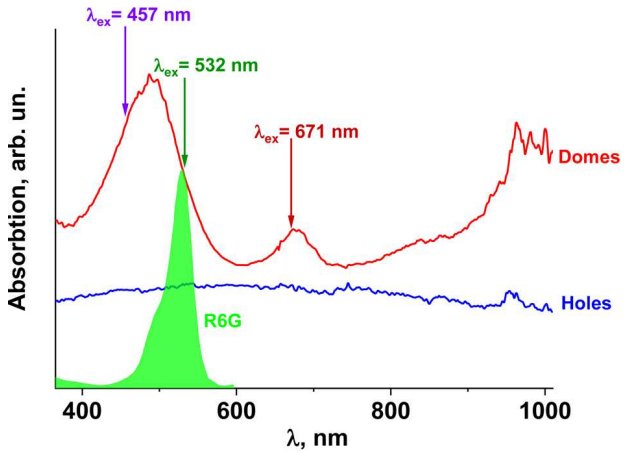

Fig. 5. Absorption spectra of bigratings with domes and holes, and the absorption spectrum of the analyte (rhodamine 6G). The arrows mark the wavelengths of laser radiation used to excite the Raman spectra

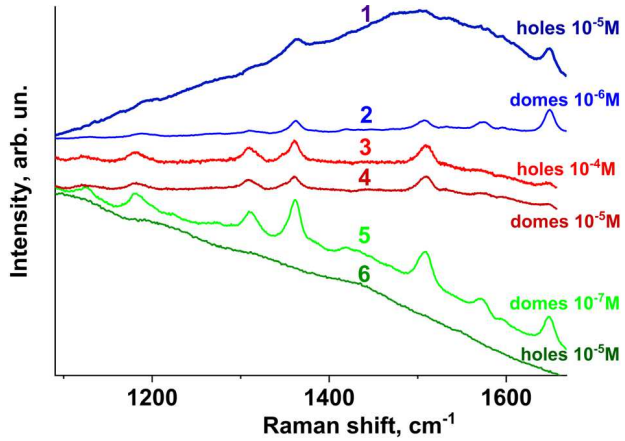

Fig. 6. Raman spectra of the standard R6G analyte with various concentrations deposited onto the SERS substrates with domes and holes. Excitation was performed by laser radiation with various wavelengths: 457 (*1* and *2*), 671 (*3* and *4*), and 532 nm (*5* and *6*)

band in the spectral interval 0.57 μm $\leq \lambda \leq$ 0.7 μm, whose spectral position practically did not change when the incidence angle was varied. This feature is typical of the LSPR excitation in metalized periodic structures [27]. Hence, it can be asserted that the studied specimens showed the excitation of both local plasmon resonances (in the matrix of domes) and plasmon-polariton surface waves (in both specimens). It is known [26] that the dependence of the SPP excitation efficiency on the quantity h/a has a maximum, i.e., there is an optimal h/a-value at which the energy transfer from the incident electromagnetic wave to the surface plasmon-polariton mode is maximum. For silver, this value equals 0.042 [28], which is significantly lower than the modulation depth of the studied specimens. Therefore, the efficiency of the SPP excitation in the researched periodic structures was low.

As mentioned above, the spectral-angular dependences of R_p, which are shown in Fig. 4, were obtained within the interval of light incidence angles from 10° to 70°. But, the Raman spectra of those SERS substrates were studied at the normal incidence of excitation radiation. Therefore, the reflection spectra of the researched specimens were measured at $\theta = 0°$ as well. In Fig. 5, the absorption spectra of bigratings with domes and holes, as well as the absorption spectrum of rhodamine 6G, are shown. The arrows point the spectral regions to which the exciting laser radiation belongs. Namely, the laser radiation with wavelengths of 457 and 532 nm had frequencies within the band of the localized plasmon resonance at the SERS substrate with domes, and the frequency of radiation with $\lambda = 671$ nm belongs to another, less intensive absorption band. Therefore, we expected that if the Raman spectra from the R6G analyte are excited by means of radiation with the indicated wavelengths, the Raman signals would be amplified. At the same time, the SERS substrate with holes was characterized by an absorption spectrum without local maxima.

Figure 6 demonstrates the Raman spectra registered at minimum concentrations of the standard R6G analyte deposited onto the SERS substrates with domes and holes, and excited by means of laser radiation with various wavelengths. As the research showed, the minimum concentration of the R6G analyte (10^{-7} M) was registered on the SERS substrate with domes if the spectrum was excited by means of radiation with $\lambda = 532$ nm. At the same time, under the same conditions, no Raman spectrum at all was registered from the SERS substrate with holes at an R6G concentration of 10^{-5} M (Fig. 6, curve *6*). On the one hand, this is a result of the absence of a local plasmon absorption band (Fig. 5) that would stimulate a considerable plasmon amplification of the Raman signal for these gratings; on the other hand, this is a manifestation of intensive photoluminescence (PL) of rhodamine 6G. Photoluminescence from R6G also manifested itself on the SERS substrate with

domes. However, a more substantial amplification of Raman modes in this case allowed us to register Raman bands against the background of intensive PL (Fig. 6, curve *5*).

When Raman spectra were excited by means of the radiation with $\lambda = 457$ nm, signals from R6G with concentrations of 10^{-6} M and 10^{-5} M were registered on the SERS substrates with domes and holes, respectively. This means that, for a reliable registration of Raman spectra on SERS substrates with holes, the R6G analyte with a concentration by an order of magnitude higher must be deposited. In this case, the Raman spectrum can be distinguished well against the intensive PL background, although not all Raman bands clearly manifest themselves (Fig. 6, curve *1*).

At the same time, it should be noted that, in the case of the SERS substrate with domes, if the spectra were excited by radiation with $\lambda = 457$ nm, the R6G analyte was registered, only if it was deposited with a concentration of 10^{-6} M, i.e., an order of magnitude higher as compared to the case where the spectra were excited by radiation with $\lambda = 532$ nm. This fact is well understood, because at $\lambda = 532$ nm, besides the plasmon amplification, there is also the amplification owing to the classical resonance Raman scattering.

When the Raman spectra from the R6G analyte were excited using radiation with $\lambda = 671$ nm, the signal amplification for both domes and holes was weaker in comparison with those described above. In this case, reliably registered were signals from R6G on the SERS substrates with domes and holes with concentrations of 10^{-5} M and 10^{-4} M, respectively. The amplification reduction of the signal from R6G by an order of magnitude when using radiation with $\lambda = 671$ nm can have two origins. First, under nonresonance conditions, if the power densities of the exciting laser radiation are identical, the intensity of the Raman signal is proportional to the fourth power of the laser radiation frequency, whence it follows that the shorter the wavelength, the higher the intensity of the Raman bands. Second, as one can see from Fig. 5, in the case of domes, the intensity of the plasmon absorption band at 671 nm is substantially lower than the intensities of the corresponding bands ar 457 and 532 nm, so the plasmon amplification of Raman signals will be substantially lower.

It is also worth noting that the morphology of the formed SERS substrates of both types does not favor the formation of hot spots. The latter can considerably enhance the amplification factor for Raman signals from analytes. To some extent, the tops of the domes can mimic them, but their surface density is very low. Therefore, in the future, it is necessary to develop substrates with the nanostructured upper metal layer.

4. Conclusions

In this work, the possibility of the formation of SERS substrates with laterally ordered domes or holes using the interference photolithography method has been demonstrated. The surface morphology of the SERS substrates was determined with the help of the AFM method. In particular, it is shown that the grating periods in both cases are equal to 1200 nm, and the depth of the holes and the height of the domes are equal to about 350 nm. The subsequent deposition of aluminum (80 nm), silver (70 nm), and gold (10 nm) layers practically did not change the depth of the holes and the height of the domes, but it led to a reduction in the holes' diameters by 10–15% and a slight (∼5%) increase in the domes' sizes.

By studying the optical properties of the manufactured structures via measuring the spectral-angular dependences of the polarized light reflection in a wavelength interval of 0.4–1.1 μm and an incidence angle interval of 10–70°, it is shown that the excitation of both local plasmon resonances (the structures with domes) and plasmon-polariton surface waves (in the structures of both types) can be observed on the formed SERS substrates.

It is demonstrated that the formed structures with laterally ordered domes and holes are effective SERS substrates, and the structures with domes enhance the Raman signal from the standard analyte R6G more efficiently (by an order of magnitude higher). This discrepancy follows from the fact that if the exciting laser radiation is normally incident on the SERS substrate, the surface of which is an ensemble of domes, localized plasmons are effectively excited in spectral intervals with maxima at 488 and 676 nm, whereas such features do not manifest themselves in the absorption spectrum of the SERS substrate with holes.

1. S.A. Meyer, E.C. Le Ru, P.G. Etchegoin. Combining surface plasmon resonance (SPR) spectroscopy with surface-enhanced raman scattering (SERS). *Anal. Chem.* **83**, 2337 (2011).

2. R. Pilot, R. Signorini, C. Durante, L. Orian, M. Bhamidipati, L. Fabris. A review on surface-enhanced Raman scattering. *Biosensors* **9**, 57 (2019).
3. C. Xiao, Z. Chen, M. Qin, D. Zhang. H. Wu. Two dimensional sinusoidal Ag nanograting exhibits polarization-independent surface-enhanced Raman spectroscopy and its surface plasmon polariton and localized surface plasmon coupling with Au nanospheres colloids. *J. Raman Spectrosc.* **50**, 1 (2018).
4. L. Lan, Y. Gao, X. Fan, M. Li, Q. Hao, T. Qiu. The origin of ultrasensitive SERS sensing beyond plasmonics. *Front. Phys.* **16**, 43300 (2021).
5. M.V. Chursanova, L.P. Germash, V.O. Yukhymchuk, V.M. Dzhagan, I.A. Khodasevich, D. Cojoc. Optimization of porous silicon preparation technology for SERS applications. *Appl. Surf. Sci.* **256**, 3369 (2010).
6. V. Cupil-Garcia, P. Strobbia, B.M. Crawford, H.-N. Wang, H. Ngo, Y, Liu, T. Vo-Dinh. Plasmonic nanoplatforms: From surface-enhanced Raman scattering sensing to biomedical applications. *J. Raman Spectrosc.* **52**, 1 (2020).
7. S. Schlucker. Surface-enhanced Raman spectroscopy: Concepts and chemical applications. *Angew. Chem. Int. Ed.* **53**, 4756 (2014).
8. W. Xie, S. Schlucker. Medical applications of surface-enhanced Raman scattering. *Phys. Chem. Chem. Phys.* **15**, 5329 (2013).
9. Z.A. Nima, A. Biswas, I.S. Bayer, F.D. Hardcastle, D. Perry, A. Ghosh, E. Dervishi, A.S. Biris. Applications of surface-enhanced Raman scattering in advanced bio-medical technologies and diagnostics. *Drug Metab. Rev.* **46**, 155 (2014).
10. P.H.B. Aoki, L.N. Furini, P. Alessio, A.E. Aliaga, C.J.L. Constantino. Surface-enhanced Raman scattering (SERS) applied to cancer diagnosis and detection of pesticides, explosives, and drugs. *Rev. Anal. Chem.* **32**, 55 (2013).
11. M. Leona, J. Stenger, E. Ferloni. Application of surface-enhanced Raman scattering techniques to the ultrasensitive identification of natural dyes in works of art. *J. Raman Spectrosc.* **37**, 981 (2006).
12. N.P.W. Pieczonka, R.F. Aroca. Single molecule analysis by surfaced-enhanced Raman scattering. *Chem. Soc. Rev.* **37**, 946 (2008).
13. W. Yue, Z. Wang, J. Whittaker, F. Lopez-royo, Y. Yangd, A.V. Zayats. Amplification of surface-enhanced Raman scattering due to substrate-mediated localized surface plasmons in gold nanodimers. *J. Mater. Chem. C* **4**, 2 (2016).
14. N. Valley, N. Greeneltch, R.P. Van Duyne, G.C. Schatz. A look at the origin and magnitude of the chemical contribution to the enhancement mechanism of surface-enhanced Raman spectroscopy (SERS): Theory and experiment. *J. Phys. Chem. Lett.* **4**, 2599 (2013).
15. Ye. Kalachyova, D. Mares, O. Lyutakov, M. Kostejn, L. Lapcak, V. Švorčík. Surface plasmon polaritons on silver gratings for optimal SERS response. *J. Phys. Chem. C* **119**, 9506 (2015).
16. D. Barchiesi, A. Otto. Excitations of surface plasmon polaritons by attenuated total reflection, revisited. *Riv. Nuovo Cim.* **36**, 173 (2013).
17. S.L. Kleinman, R.R. Frontiera, A.-I. Henry, J.A. Dieringer, R.P. Van Duyne. Creating, characterizing, and controlling chemistry with SERS hot spots. *Phys. Chem. Chem. Phys.* **15**, 21 (2013).
18. V.O. Yukhymchuk, S.A. Kostyukevych, V.M. Dzhagan, A.G. Milekhin, E.E. Rodyakina, I.B. Yanchuk, P.Ye. Shepeliavy, M.Ya. Valakh, K.V. Kostyukevych, V.O. Lysiuk, I.V. Tverdokhlib. SERS of Rhodamine 6G on substrates with laterally ordered and random gold nanoislands. *Semicond. Phys. Quant. Electron. Optoelectron.* **15**, 232 (2012).
19. M.V. Chursanova, V.M. Dzhagan, V.O. Yukhymchuk, O.S. Lytvyn, M.Y. Valakh, I.A. Khodasevich, D. Lehmann, D.R.T. Zahn, C. Waurisch, S.G. Hickey. Nanostructured silver substrates with stable and universal SERS properties: application to organic molecules and semiconductor nanoparticles. *Nanosc. Res. Lett.* **5**, 403 (2010).
20. V.O. Yukhymchuk, O.M. Hreshchuk, V.M. Dzhagan, M.V. Sakhno, M.A. Skoryk, S.R Lavoryk, G.Y. Rudko, N.A. Matveevskaya, T.G. Beynik, M.Ya. Valakh. Experimental studies and modeling of "starlike" plasmonic nanostructures for SERS application. *Phys. Status Solidi B* **256**, 1800280 (2019).
21. V. Dan'ko, M. Dmitruk, I. Indutnyi, S. Mamykin, V. Myn'ko, M. Lukaniuk, P. Shepeliavyi, P. Lytvyn. Fabrication of periodic plasmonic structures using interference lithography and chalcogenide photoresist. *Nanosc. Res. Lett.* **10**, 497 (2015).
22. I.Z. Indutnyy, M. Popescu, A. Lorinczi, F. Sava, V.I. Min'ko, P.E. Shepeliavyi, V.A. Dan'ko. Fabrication of submicrometer periodic structures using interference lithography and two-layer chalcogenide photoresist. *J. Optoelectron. Adv. Mater.* **11**, 1967 (2009).
23. V.A. Dan'ko, I.Z. Indutnyi, V.I. Mynko, P.M. Lytvyn, M.V. Lukaniuk, H.V. Bandarenka, A.L. Dolgyi, S.V. Redko. Formation of laterally ordered arrays of noble metal nanocavities for SERS substrates by using interference photolithography. *Semicond. Phys. Quant. Electron. Optoelectron.* **24**, 48 (2021).
24. N.L. Dmitruk, V.G. Litovchenko, V.L Strygewskyy. *Surface Polaritons in Semiconductors and Dielectrics* (Naukova Dumka, 1989).
25. P.B. Johnson, R.W. Christy. Optical constants of the noble metals. *Phys. Rev. B* **6**, 4370 (1972).
26. I.Z. Indutny, V.I. Minko, M.V. Sopinskyi, V.A. Danko, P.M. Lytvyn, A.A. Korchovyi. Dependence of the excitation efficiency of surface plasmon-polaritons on the relief depth of aluminum lattice. *Optoelektron. Polyprov. Tekhn.* **55**, 117 (2020) (in Ukrainian).
27. M.V. Sosnova, N.L. Dmitruk, A.V. Korovin, S.V. Mamykin. Local plasmon excitations in one-dimensional array of metal nanowires for sensor applications. *Appl. Phys. B* **99**, 493 (2010).